Radiat Detect Technol Methods (2018) 2:2
https://doi.org/10.1007/s41605-017-0027-x

ORIGINAL PAPER

The next generation of crystal detectors

Ren-Yuan Zhu[1]

Received: 29 August 2017 / Revised: 27 October 2017 / Accepted: 30 October 2017

Abstract
Background In high-energy and nuclear physics experiments, total absorption electromagnetic calorimeters made of inorganic crystals are known for their superb energy resolution and detection efficiency for photon and electron measurements. A crystal calorimeter is thus the choice for those experiments where precision measurements of photons and electrons are crucial for their physics missions. It is also known that the existing crystal detectors are neither bright nor fast enough nor radiation hard enough to survive severe radiation environment expected in future HEP experiments. Crystal detectors have also been proposed to build a homogeneous hadron calorimeter to achieve unprecedented jet mass resolution by duel readout of both Cherenkov and scintillation light, where the development of cost-effective crystal detectors is a crucial issue because of the 100 cubic meters crystal volume required.
Purpose To develop novel inorganic crystal scintillator-based detector concepts for future HEP experiments at the energy and intensity frontiers.
Methods Optical and scintillation properties of novel inorganic crystal scintillators, such as excitation, emission and transmittance spectra, light output and decay time, are characterized before and after irradiation by ionization dose and hadrons. Their performance and radiation hardness are compared to the requirements, and feedback is given to the crystal manufacturers for quality improvement.
Results As a result of this investigation, several inorganic crystal scintillator-based detector concepts are established for future HEP experiments, such as an LSO/LYSO crystal-based total absorption and/or sampling calorimeter concept, a barium fluoride crystal-based very fast crystal calorimeter concept, and a cost-effective inorganic scintillator-based homogeneous hadron calorimeter concept.
Conclusion Bright, fast and radiation hard LYSO/LSO crystals may be used for a total absorption ECAL. An LYSO/W Shashlik sampling calorimeter will survive the harsh radiation environment expected at the HL-LHC. With sub-ns decay time of its fast scintillation component and excellent radiation hardness, barium fluoride crystals would provide more than ten times faster rate and timing capability, provided that their slow scintillation component is effectively suppressed to avoid pileup. PbF2, PbFCl and BSO crystals may provide a foundation for a homogeneous hadron calorimeter with dual readout for both Cherenkov and scintillation light to achieve unprecedented jet mass resolution for future lepton colliders.

Keywords Crystal · Scintillator · Calorimeter · Radiation damage · Fast timing · Dual readout

Introduction

Crystal detectors have been used widely in high-energy and nuclear physics experiments, medical instruments and homeland security applications. Novel crystal detectors are continuously being discovered and developed in academia and industry.

In high-energy physics (HEP) and nuclear physics (NP) experiments, total absorption electromagnetic calorimeters (ECALs) made of inorganic crystals are known for their superb energy resolution and detection efficiency for pho-

✉ Ren-Yuan Zhu
zhu@hep.caltech.edu

[1] 256-48, HEP, California Institute of Technology, Pasadena, CA 91125, USA

Published online: 01 December 2017

Table 1 Existing crystal calorimeters in high-energy physics

Date	75-85	80-00	80-00	80-00	90-10	94-10	94-10	95-20
Experiment	C. Ball	L3	CLEO II	C. Barrel	KTeV	BaBar	BELLE	CMS
Accelerator	SPEAR	LEP	CESR	LEAR	FNAL	SLAC	KEK	CERN
Crystal type	NaI:Tl	BGO	CsI:Tl	CsI:Tl	CsI	CsI:Tl	CsI:Tl	PWO
B-Field (T)	–	0.5	1.5	1.5	–	1.5	1.0	4.0
r_{inner} (m)	0.254	0.55	1.0	0.27	–	1.0	1.25	1.29
Crystal number	672	11,400	7800	1400	3300	6580	8800	76,000
Crystal depth (X_0)	16	22	16	16	27	16–17.5	16.2	25
Crystal volume (m^3)	1	1.5	7	1	2	5.9	9.5	11
Light output (p.e./MeV)	350	1400	5000	2000	40	5000	5000	2
Photodetector	PMT	Si PD	Si PD	WS+Si PD	PMT	Si PD	Si PD	Si APD
Gain of photodetector	Large	1	1	1	4000	1	1	50
σ_N/Channel (MeV)	0.05	0.8	0.5	0.2	Small	0.15	0.2	40
Dynamic range	10^4	10^5	10^4	10^4	10^4	10^4	10^4	10^5

ton and electron measurements [1]. A crystal ECAL is thus the choice for those experiments where precision measurements of photons and electrons are crucial for their physics missions. Examples are the Crystal Ball NaI:Tl ECAL, the L3 BGO ECAL and the BaBar CsI:Tl ECAL in lepton colliders, the kTeV CsI ECAL and the CMS PWO ECAL in hadron colliders and the Fermi CsI:Tl ECAL in space. Table 1 lists existing crystal calorimeters in high-energy physics.

For future HEP experiments at the energy and intensity frontiers, however, the crystal detectors used in the above-mentioned ECALs are either not bright and fast enough, or not radiation hard enough. Crystals have also been proposed to build a homogeneous hadron calorimeter (HHCAL) to achieve unprecedented jet mass resolution by duel readout of both Cherenkov and scintillation light [2], where development of cost-effective crystal detectors is a crucial issue because of the huge crystal volume required [3]. This paper discusses several R&D directions for the next-generation crystal detectors for future HEP experiments.

Performance of PWO crystals

Table 1 shows that the CMS lead tungstate ($PbWO_4$ or PWO) crystal calorimeter, consisting of 76,000 crystals of 11 m^3, is the largest crystal calorimeter ever built. Because of its superb energy resolution and detection efficiency, the CMS PWO ECAL has played an important role for the discovery of the Higgs boson by the CMS experiment [4]. One crucial issue is crystal's radiation damage in the severe radiation environment at LHC, which requires precision monitoring to correct variations of crystal transparency [5]. After 2 years of operation, up to 70% loss of light output was observed in the CMS PWO crystals at large rapidity in situ at LHC as shown in Fig. 1 when the LHC was running at a luminosity of

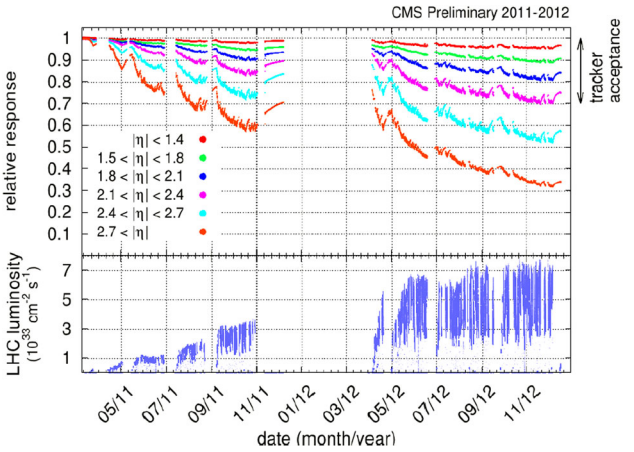

Fig. 1 Monitoring response of CMS PWO crystals observed during LHC run I

up to 5×10^{33} cm^{-2} s^{-1} and a half of its designed energy [6]. The damage in PWO crystals increases when the luminosity increases, and recovers during LHC stops.

The radiation damage of PWO crystals shown in Fig. 1 is well understood. It is caused by radiation induces absorption, or color center formation, and is dose rate dependent [7]. Figure 2 shows that light output of a PWO crystal reached an equilibrium during irradiation under a defined dose rate, indicating a dose rate-dependent radiation damage caused by color center dynamics. At equilibrium the speed of the color center formation (damage) equals to the speed of the color center annihilation (recovery), so that the color center density, or the radiation-induced absorption, does not change unless the applied dose rate changes [7].

Figure 3 shows emission-weighted radiation-induced absorption coefficient (EWRIAC) as a function of the γ-ray dose rate measured for a batch of mass-produced BTCP PWO crystals [8]. The EWRIAC values of all crystals are less

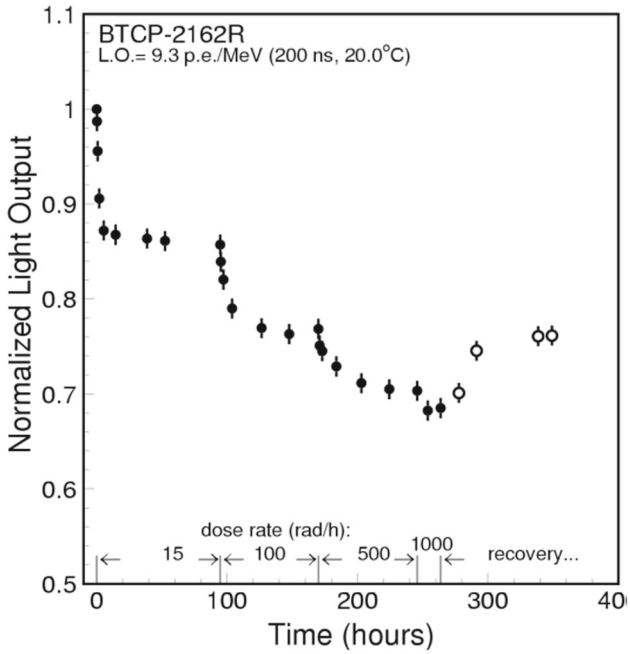

Fig. 2 Dose rate-dependent light output loss observed in a PWO crystal

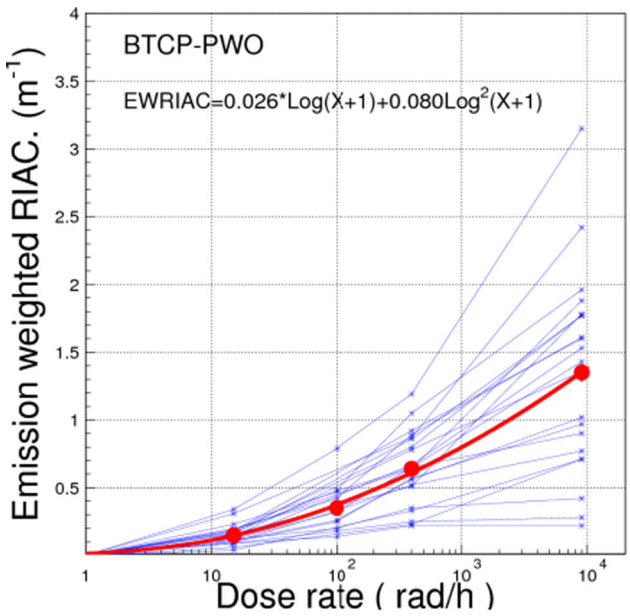

Fig. 3 EWRIAC values are shown as a function of dose rate for mass-produced PWO

than $1\,m^{-1}$ up to $400\,rad\,h^{-1}$, indicating no damage to the light response uniformity for PWO crystals used in the CMS ECAL barrel, where the maximum dose rate is expected to be a few hundreds $rad\,h^{-1}$ even if the LHC luminosity is increased by a factor of ten, e.g., at HL-LHC. The EWRIAC values measured at $9000\,rad\,h^{-1}$, however, are diverse. Some samples show up to $3\,m^{-1}$, indicating possible damages in the light response uniformity and thus the energy resolution.

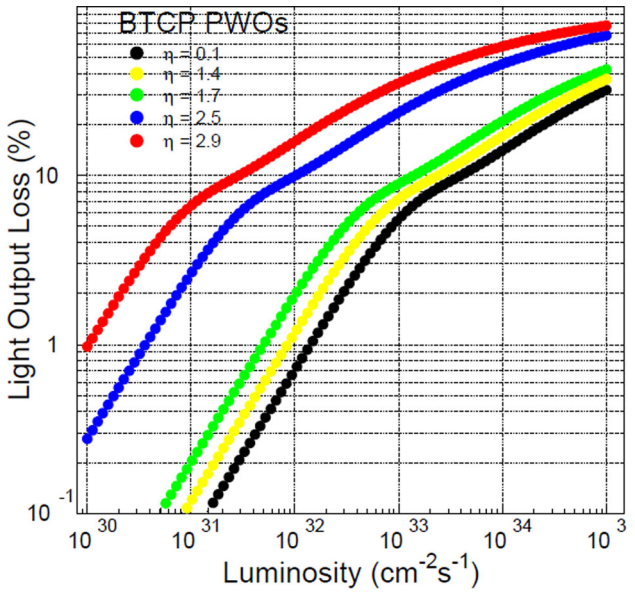

Fig. 4 Predicated light output loss as a function of luminosity and rapidity

Figure 4 shows the expected light output loss as a function of luminosity for PWO crystals at different rapidity predicted in 2010 before LHC running [9]. This prediction was made according to the measured relation between light output and radiation-induced absorption assuming the average EWRIAC values shown in red color in Fig. 3. A detailed comparison shows that this prediction agrees well with the data shown in Fig. 1, indicating that radiation damage in PWO crystals observed so far is caused by ionization dose.

Additional damage caused by charged hadrons was also studied [10]. Because of these damages, the CMS endcap PWO ECAL is proposed to be replaced by using more radiation hard technologies [11], one of which is a LYSO crystal-based Shashlik sampling calorimeter [12].

Radiation hard LYSO/LSO crystals

Because of their high density ($7.4\,g\,cm^{-3}$), short radiation length (1.14 cm), fast (40 ns) and bright (4 times BGO) scintillation, cerium-doped lutetium oxyorthosilicate (Lu_2SiO_5:Ce, LSO) [13] and lutetium yttrium oxyorthosilicate ($Lu_{2(1-x)}Y_{2x}SiO_5$:Ce, LYSO) [14,15] crystals have attracted a broad interest in the high-energy physics community pursuing precision electromagnetic calorimeter for future high-energy physics experiments [12,16–19]. Their excellent radiation hardness against gamma rays [15,20], neutrons [17] and charged hadrons [10] also makes them a preferred material for calorimeters to be operated in a severe radiation environment, such as the HL-LHC.

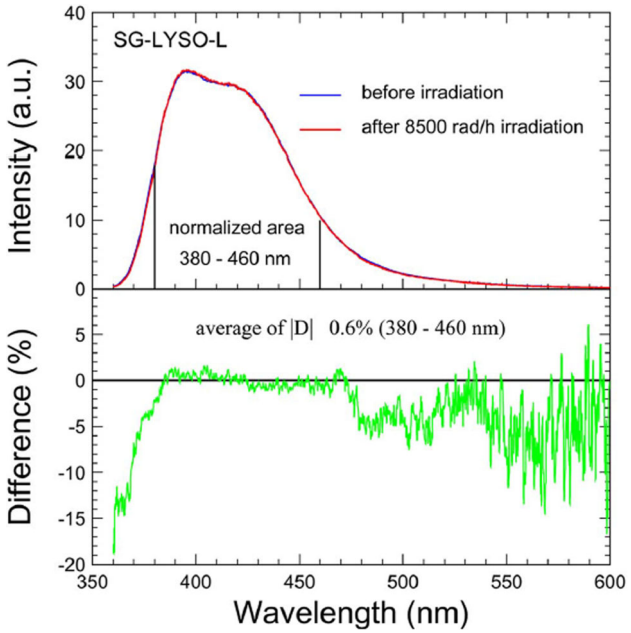

Fig. 5 Photoluminescence of a LYSO crystal before and after 1 Mrad γ-ray irradiation

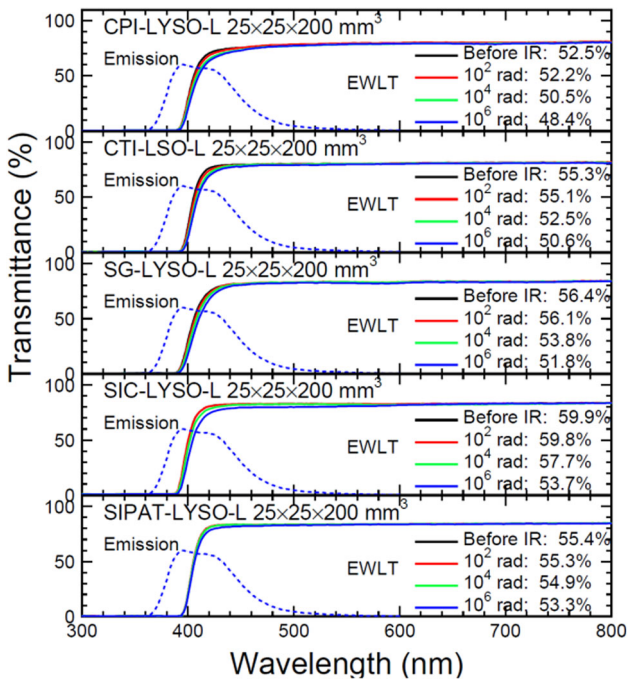

Fig. 6 LT of 20-cm-long LYSO crystals before and after irradiations

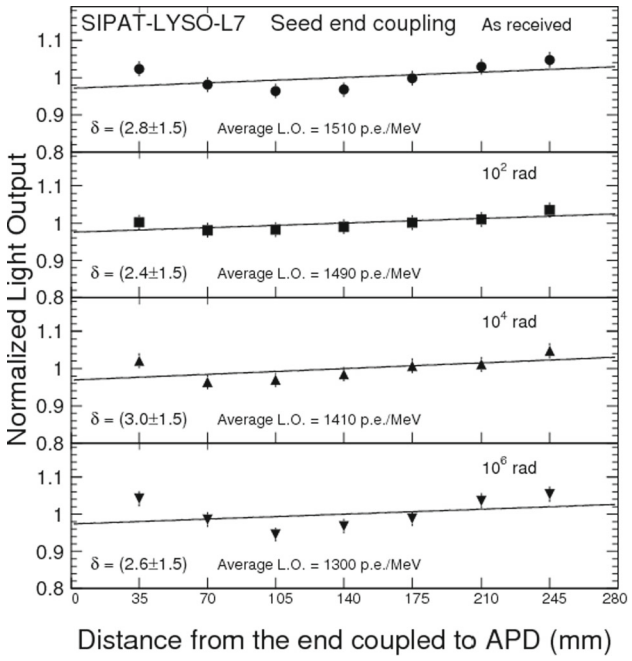

Fig. 7 LO and LRU measured by APD for a 28-cm-long SIPAT LYSO crystal

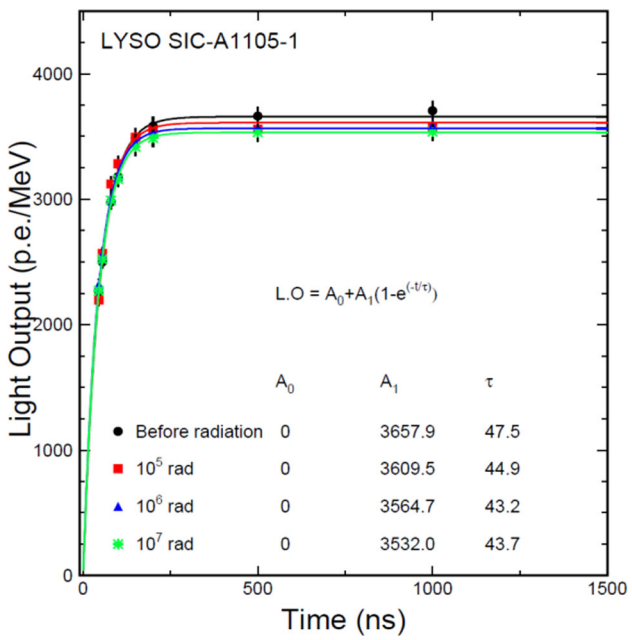

Fig. 8 LO and decay kinetics measured by PMT for an SIC LYSO plate

The top plot of Fig. 5 shows the photoluminescence spectra of a LYSO crystal measured before (blue) and after (red) 1 Mrad γ-ray irradiation [20]. To facilitate a comparison, these spectra were normalized to the area between 380 and 460 nm under the spectra. The corresponding relative difference is shown in the bottom plot of Fig. 5. The bin-by-bin average of the absolute difference between the spectra measured before and after the irradiation is found to be 0.6% in the normalization region, less than the systematic uncertainty for this measurement. This indicates that the γ-ray irradiation does not affect the scintillation mechanism in LYSO crystals.

Figure 6 shows the longitudinal transmittance spectra for five 200-mm-long LYSO crystals from different vendors before and after several steps of the γ-ray irradiation

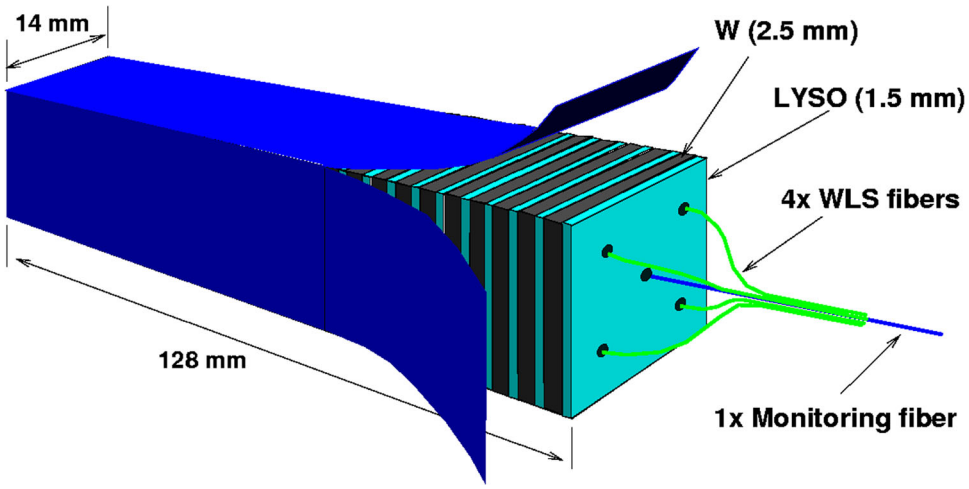

Fig. 9 A schematic showing a LYSO/W Shashlik calorimeter concept consisting of LYSO plates of 1.5 mm thick and tungsten plates of 2.5 mm thick, 4 WLS fibers and one monitoring fiber

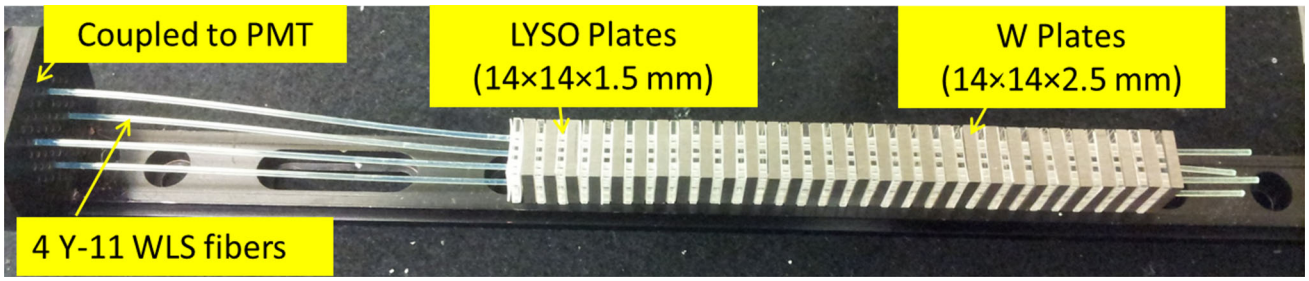

Fig. 10 A photograph showing a LYSO/W Shashlik tower with four WLS fibers inserted

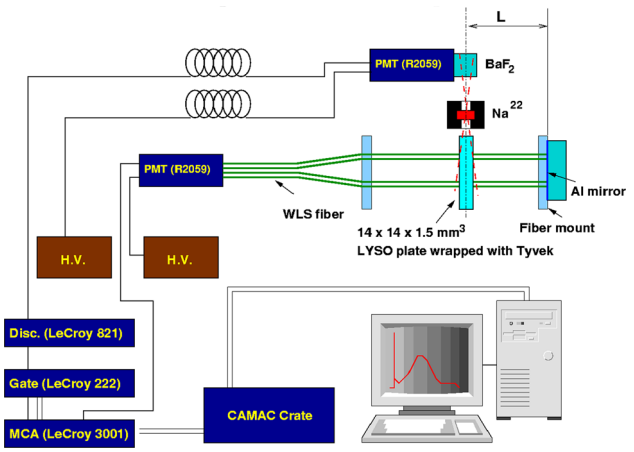

Fig. 11 A setup used to measure the longitudinal uniformity for a LYSO/W Shashlik tower

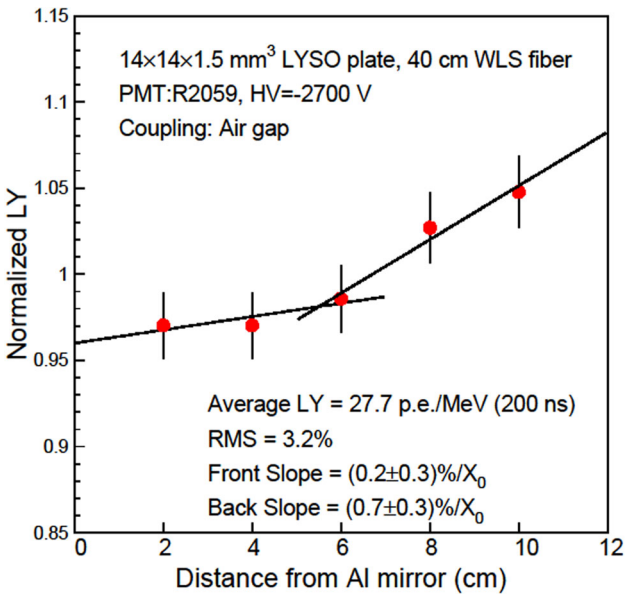

Fig. 12 Longitudinal response uniformity of a LYSO/W Shashlik tower

with integrated dose of 10^2, 10^4 and 10^6 rad. Also shown in the figure are the corresponding numerical values of the photoluminescence-weighted longitudinal transmittance (EWLT), which is defined as:

$$\mathrm{EWLT} = \frac{\int \mathrm{LT}(\lambda)\mathrm{Em}(\lambda)\mathrm{d}\lambda}{\int \mathrm{Em}(\lambda)\mathrm{d}\lambda}. \quad (1)$$

EWLT represents crystal's transparency better than the transmittance at the emission peak since it runs through the entire emission spectrum. This is particularly important for crystals with self-absorption nature, i.e., a part of scintillation

Table 2 Basic Properties of fast crystal scintillators

	LSO/LYSO	GSO	YSO[1]	CsI	BaF_2	CeF_3	$CeBr_3$[2]	$LaCl_3$	$LaBr_3$	Plastic scintillator (BC 404)[3]
Density (g/cm^3)	7.40	6.71	4.44	4.51	4.89	6.16	5.23	3.86	5.29	1.03
Melting point (°C)	2050	1950	1980	621	1280	1460	722	858	783	70#
Radiation Length (cm)	1.14	1.38	3.11	1.86	2.03	1.70	1.96	2.81	1.88	42.54
Mollière Radius (cm)	2.07	2.23	2.93	3.57	3.10	2.41	2.97	3.71	2.85	9.59
Interaction Length (cm)	20.9	22.2	27.9	39.3	30.7	23.2	31.5	37.6	30.4	78.8
Z value	64.8	57.9	33.3	54.0	51.6	50.8	45.6	47.3	45.6	–
dE/dX (MeV/cm)	9.55	8.88	6.56	5.56	6.52	8.42	6.65	5.27	6.90	2.02
Emission Peak[a] (nm)	420	430	420	310	300 220	340 300	371	335	356	408
Refractive Index[b]	1.82	1.85	1.80	1.95	1.50	1.62	1.9	1.9	1.9	1.58
Relative Light Yield[a,c]	100	45	76	4.2 1.3	42 4.8	8.6	141	15 49	153	35
Decay Time[a] (ns)	40	73	60	30 6	650 0.9	30	17	570 24	20	1.8
d(LY)/dT [d] (%/°C)	–0.2	–0.4	–0.3	–1.4	–1.9 0.1	~0	-0.1	0.1	0.2	~0

a. Top line: slow component, bottom line: fast component.
b. At the wavelength of the emission maximum.
c. Relative light yield normalized to the light yield of LSO
d. At room temperature (20°C)
#. Softening point

1. N. Tsuchida et al ***Nucl. Instrum. Methods Phys. Res. A,*** 385 (1997) 290-298
http://www.hitachi-chem.co.jp/english/products/cc/017.html
2. W. Drozdowski et al. ***IEEE TRANS. NUCL. SCI***, VOL.55, NO.3 (2008) 1391-1396
Chenliang Li et al, ***Solid State Commun***, Volume 144, Issues 5–6 (2007),220–224
http://scintillator.lbl.gov/
3 . http://www.detectors.saint-gobain.com/Plastic-Scintillator.aspx
http://pdg.lbl.gov/2008/AtomicNuclearProperties/HTML_PAGES/216.html

The red, blue, green and yellow background colors used in the table distinguish oxides (LSO, LYSO, GSO, YSO), halides (CsI, BaF_2 and CeF_3), heavily hygroscopic halides ($CeBr_3$, $LaCl_3$ and $LaBr_3$) and plastic scintillators

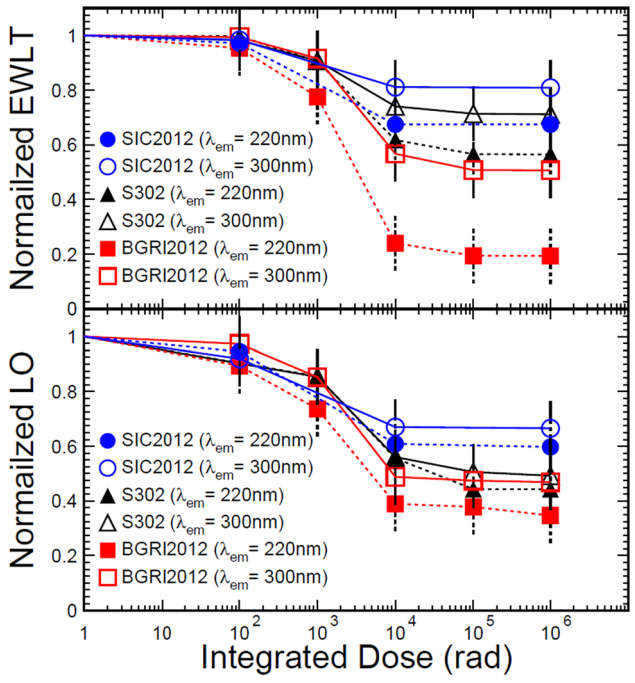

Fig. 13 Normalized EWLT and LO as a function of integrated dose for 3 BaF_2 crystals

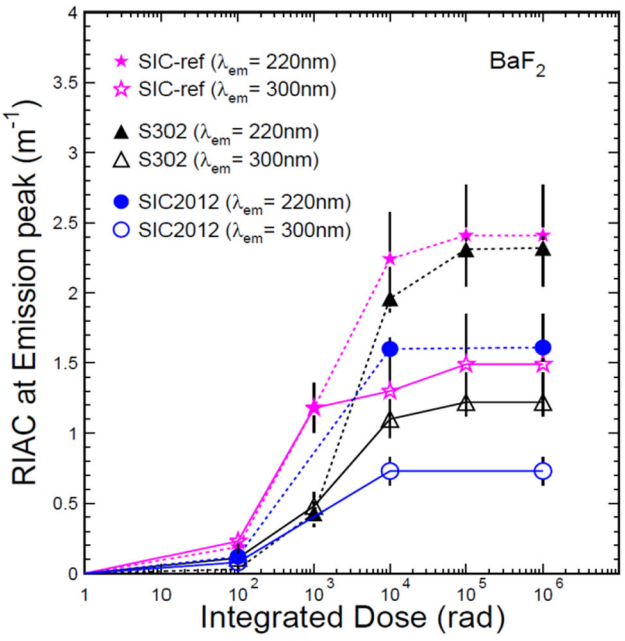

Fig. 14 RIAC as a function of integrated dose for three long BaF_2 crystals

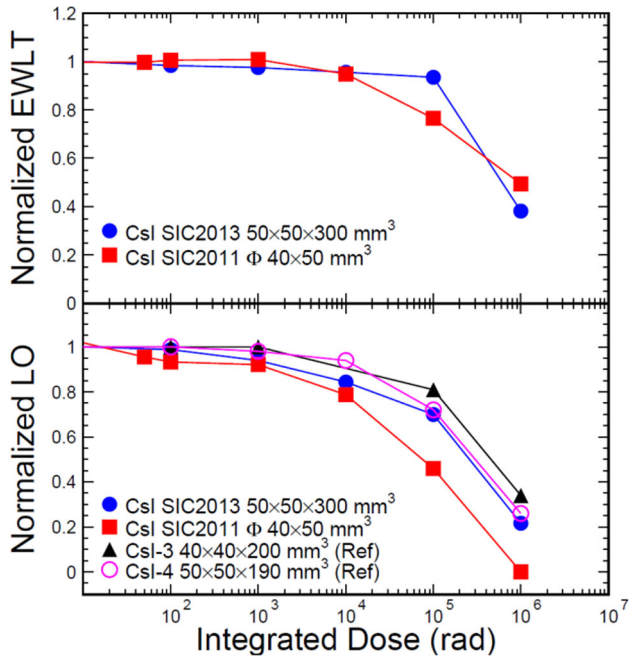

Fig. 15 Normalized EWLT and LO as a function of integrated dose for 3 CsI crystals

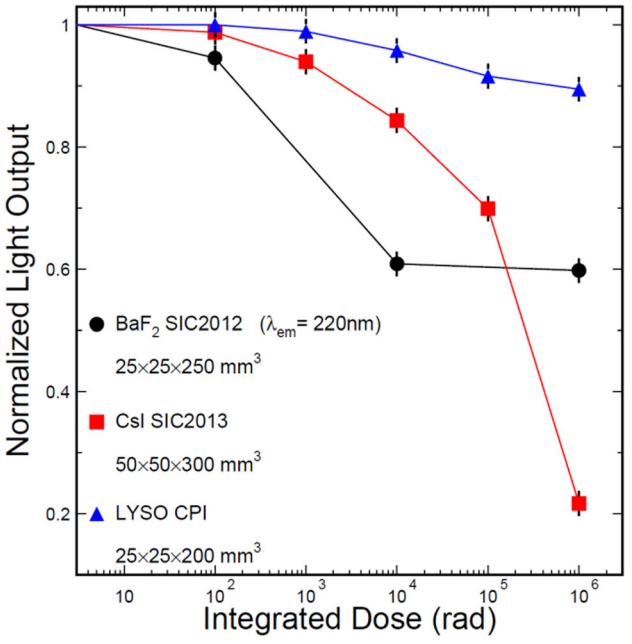

Fig. 17 Normalized EWLT and LO as a function of dose for BaF2, CsI and LYSO

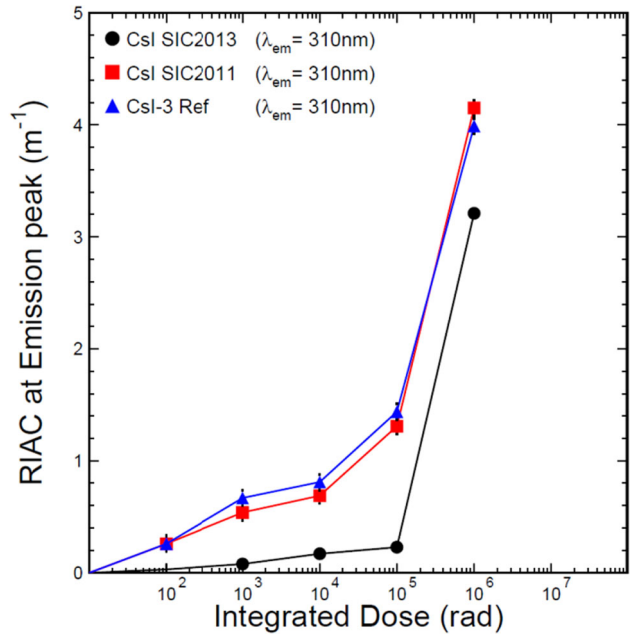

Fig. 16 RIAC as a function of integrated dose for three CsI crystals

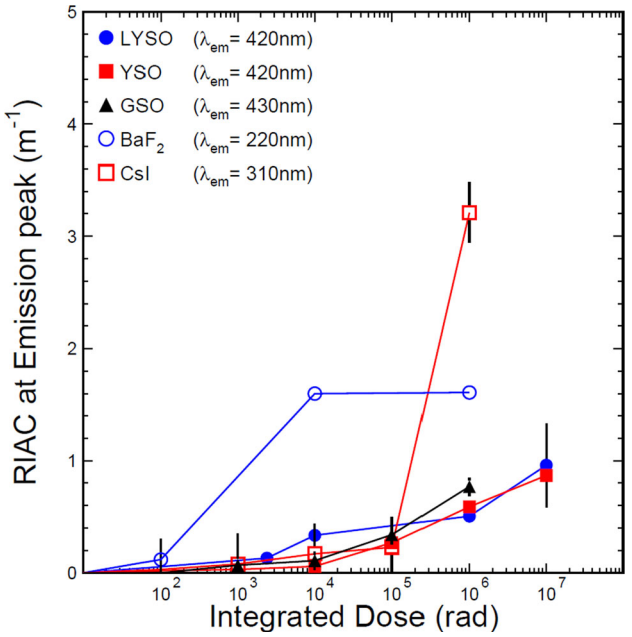

Fig. 18 RIAC as a function of integrated dose for crystals with dose rate-independent damage

is self-absorbed in the crystal [17]. Consistent damages are observed on the longitudinal transmittance of all LYSO crystal samples. It is noted that the degradation of longitudinal transmittance is small even after 10^6 rad.

Figure 7 shows light output (LO) and light response uniformity (LRU) for a 280-mm-long LYSO crystal before and after several steps of the γ-ray irradiations with integrated dose of 10^2, 10^4 and 10^6 rad [21]. About 14% LO loss is observed after 1 Mrad irradiation with LRU maintained. Figure 8 shows LO and decay time for a LYSO plate of $25 \times 25 \times 5$ mm grown by Shanghai Institute of Ceramics (SIC) before and after several steps of the γ-ray irradiations with integrated dose of 10^5, 10^6 and 10^7 rad. A LO degradation of 3.4% was observed after 10 Mrad, indicating significant reduction in radiation damage because of short

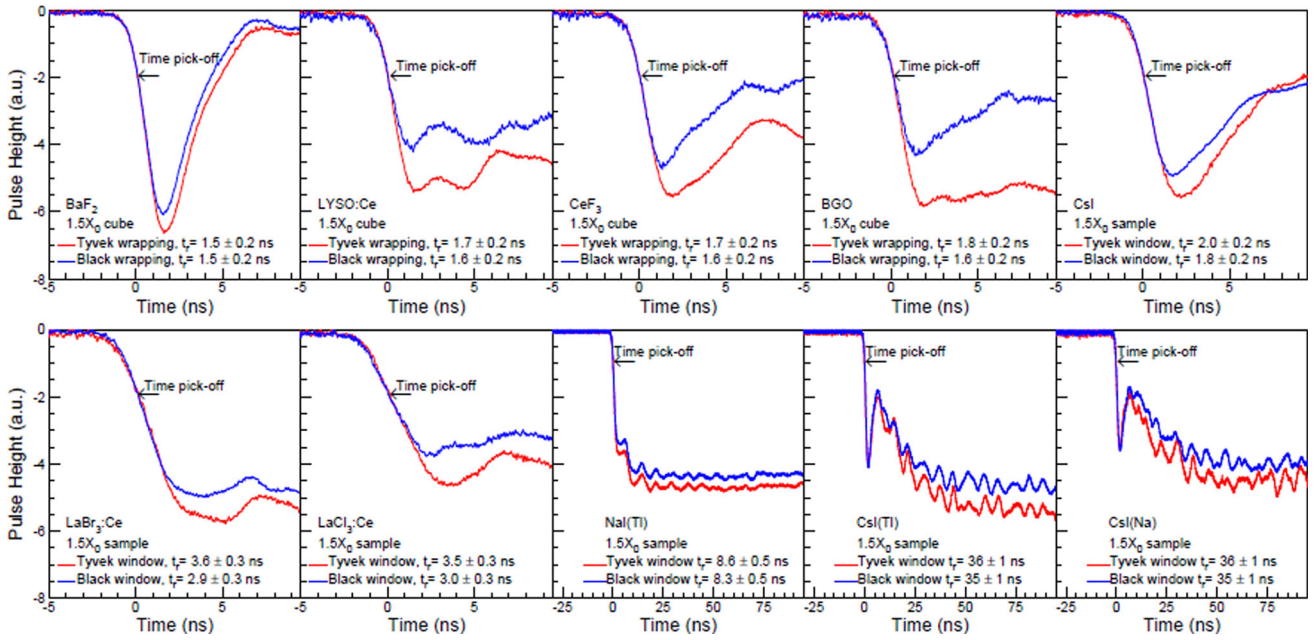

Fig. 19 Scintillation rising time measured for ten crystal samples of 1.5 X_0

light path. These results as well as the irradiation by 24 GeV protons of up to a fluence of 10^{14} cm^{-2} [10] demonstrate the excellent radiation hardness of LYSO crystals.

Figure 9 shows a LYSO crystal-based Shashlik calorimeter detector concept with four evenly distributed wavelength shifting (WLS) fibers for readout and a monitoring fiber at the center [12]. This detector concept reduces the crystal volume and cost, and improves the radiation hardness of the calorimeter because of the much reduced light path. As shown in Fig. 9, the initial design consists of 30 LYSO plates of 1.5 mm thick and 29 W plates of 2.5 mm thick. Each tower has a depth of 25 X_0 to accommodate electrons and photons with energies up to the TeV range. The sampling fraction was chosen to be around 20% to provide an adequate stochastic term of the energy resolution at a level of 10%. Because of the high density of both the LSO/LYSO crystals and the absorber materials, the average radiation length (0.51 cm) and Moliere radius (1.3 cm) are much smaller as compared to commonly used crystal scintillators. This detector concept thus also provides a very compact calorimeter to mitigate the pileup effect expected at the HL-LHC. Figure 10 shows a photograph of LYSO/W Shashlik tower with four Y-11 WLS fibers coupled to a readout PMT. Beam tests for a LYSO/W Shashlik matrix consisting of sixteen towers were carried out at Fermilab and CERN with result reported in the Proceedings of the Calor 2016 conference at Daegu, South Korea.

Figure 11 shows a setup used to measure longitudinal response uniformity for the LYSO/W Shashlik detector concept. A $14 \times 14 \times 1.5\,\text{mm}^3$ LYSO plate was moved along four Y-11 WLS fibers at five points of 2 cm apart. The LO was measured by using a γ-ray source shooting to the LYSO plate. Figure 12 shows the measured result and the corresponding fit for two straight lines using first and last three points. The corresponding slope of the fit is $0.2\%/X_0$ at the front, which is less than $0.3\%/X_0$ required to maintain good energy resolution [22]. The slope at the back is $0.7\%/X_0$, which is close to the optimum of 8% rise required in the last 10 X_0.

Alternative fast crystals

The high cost of LYSO crystals caused by high Lu_2O_3 price, however, may limit their use in future HEP experiments. Table 2 lists basic optical scintillation properties for alternative fast crystal detectors with scintillation decay time ranged from sub-nanosecond to a few tens nanosecond, and compared to plastic scintillator. Among the fast crystals listed in Table 2, mass production cost of barium fluoride (BaF_2) and pure CsI crystals is significantly lower than others because of their low raw material cost and low melting point. At this point, BaF_2 is baselined for the Mu2e experiment with pure CsI as an alternative option [23]. For applications in severe radiation environment, such as HL-LHC, one of the crucial issues for their application is radiation hardness. Investigation of radiation hardness for alternative fast crystals would provide important input for future HEP experiments at the energy and intensity frontiers. On the other hand, cost-effective fast scintillating glass and ceramics may also be considered and developed.

Figure 13 shows normalized emission-weighted longitudinal transmittance (EWLT, top) and light output (LO, bottom) as a function of integrated γ-ray dose for three 250-mm-long BaF_2 crystals. While SIC2012 and BGRI2012 were grown by SIC and Beijing Glass Research Institute (BGRI), respectively, in 2012, the crystal S302 was grown by SIC 20 years ago during nineties for the SSC. The result shows that SIC2012 is more radiation hard than other samples, indicating an improvement in crystal quality. It was also found that the slow component (300 nm) of all crystals is more radiation hard than the fast component (220 nm). BaF_2 crystals also show stable damage after 10 krad, indicating limited defect density in these crystals which was fully exhausted after 10 krad. This promises a stable BaF_2 crystal calorimeter in a severe radiation environment. Figure 14 shows radiation-induced absorption coefficient (RIAC) as a function of integrated dose for three BaF_2 crystals, indicating that RIAC of mass-produced BaF_2 may be controlled to less than 1.6 m^{-1} for the fast component. Note, RIAC is independent of sample size, so can be compared to other crystals.

Radiation hardness of large size pure CsI crystals

Figure 15 shows normalized EWLT and LO as a function of integrated γ-ray dose for large size CsI crystals. SIC2013 (30 cm long) and SIC2011 were grown by SIC in 2013 and 2011, respectively. The crystals CsI-3 (20 cm long) and CsI-4 (19 cm long) were grown by the Institute for Single Crystals, Kharkov, Ukraine. Consistent radiation damage between these crystals is observed. Figure 15 also shows that radiation damage in CsI is small below 10 krad, but degrades continuously with no sign of saturation at high dose, indicating high defect density in the crystals. Figure 16 shows RIAC as a function of integrated dose, which is longer than 3 m^{-1} after 1 Mrad.

Comparison of radiation hardness between BaF_2, pure CsI and LYSO

Figures 17 and 18 show normalized EWLT, LO and RIAC as a function of integrated dose for crystals with dose rate-independent radiation damage, i.e., BaF_2, pure CsI and LYSO. Because of no recovery, these crystals promise a more stable calorimeter than that with dose rate-dependent radiation damage, such as PWO. LYSO crystals show clearly the best radiation hardness. Among two crystals of low cost, the radiation hardness of BaF_2 is good at high dose and that of CsI is good at low dose.

Time resolution of crystal scintillation

Crystal time resolution is important for many applications. It depends on the signal-to-noise ratio for the rise time mea-

Table 3 Figure of merit for time resolution for various crystal scintillators

Crystal scintillators	Relative LY (%)	A_1 (%)	τ_1 (ns)	A_2 (%)	τ_2 (ns)	Total LO (p.e./MeV, XP2254B)	LO in 1 ns (p.e./MeV, XP2254B)	LO in 0.1 ns (p.e./MeV, XP2254B)	LY in 0.1 ns (photons/MeV)
BaF_2	40.1	91	650	9	0.9	1149	71.0	11.0	136.6
LSO:Ca,Ce	94	100	30			2400	78.7	8.0	110.9
LSO/LYSO:Ce	85	100	40			2180	53.8	5.4	75.3
CeF_3	7.3	100	30			208	6.8	0.7	8.6
BGO	21	100	300			350	1.2	0.1	2.5
PWO	0.377	80	30	20	10	9.2	0.42	0.04	0.4
$LaBr_3$:Ce	130	100	20			3810	185.8	19.0	229.9
$LaCl_3$	55	24	570	76	24	1570	49.36	5.03	62.5
NaI:Tl	100	100	245			2604	10.6	1.1	14.5
CsI	4.7	77	30	23	6	131	7.9	0.8	10.6
CsI:Tl	165	100	1220			2093	1.7	0.2	4.8
CsI:Na	88	100	690			2274	3.3	0.3	4.5

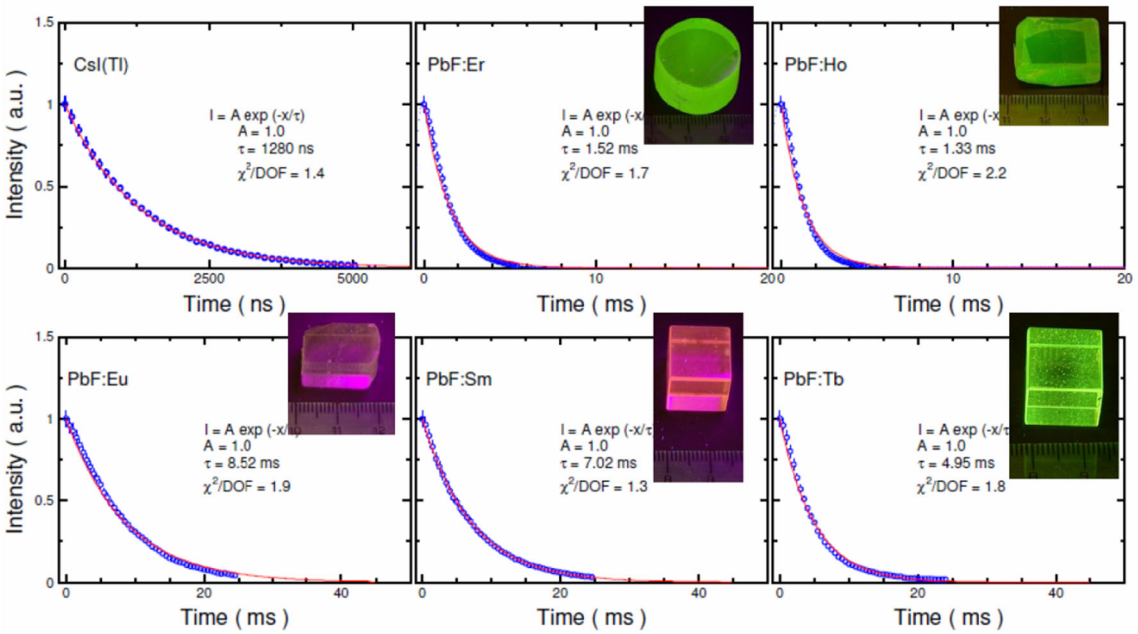

Fig. 20 Decay kinetics of doped PbF_2 exited by UV light

surement. While scintillation light is known to have very different decay time for various crystals, the intrinsic rising time of most crystals is as fast as tens ps [24]. Figure 19 shows the rising time measured by using a Hamamatsu R2059 PMT for ten crystal samples of 1.5 X_0 size. The fast rise time of about 1.5 ns observed for BaF_2, LYSO, CeF_3 and BGO is dominated by the PMT rise time 1.3 ns (2500 V) and the rise time of 0.14 ns of the Agilent MSO9254A (2.5 GHz) DSO. The measured rise time values are also reduced for the same crystal with black wrapping, indicating effect of the light propagation in the crystal [25]. We notice a 3 ns FWHM pulse width from BaF_2 crystal is the narrowest among all crystal scintillators, which may be reduced by using a aster photodetector.

Table 3 lists the values of the figure of merit for time resolution for various crystal detectors, which is defined as the light output in the 1st, or the 1st 0.1 ns [25]. It is clear that the best crystal scintillators for ultra-fast timing are BaF_2, LSO:Ca,Ce and LSO/LYSO:Ce. $LaBr_3$ is a material with high potential theoretically, but suffers from scattering centers in the crystal as well as its intrinsic hygroscopicity.

Crystals for the HHCAL detector concept

Aiming at the best jet mass resolution, cost-effective inorganic crystal scintillators are being developed for a homogeneous hadron calorimeter (HHCAL) detector concept with dual readout of both Cherenkov and scintillation light for future high-energy lepton colliders [2]. Because of the unprecedented volume (70–100 m^3) foreseen for the HHCAL

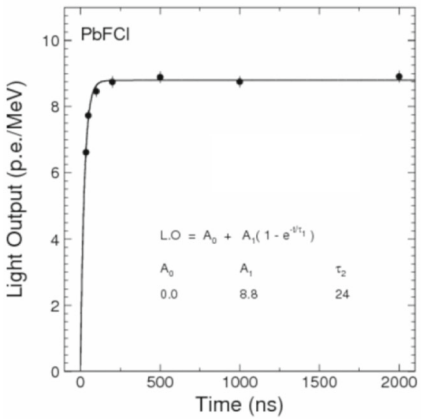

Fig. 21 Decay kinetics of a PbFCl sample excited by γ-rays

detector concept, cost-effectiveness is the most important requirement [3]. In addition, the material must be dense to reduce the calorimeter volume, UV transparent for effective collection of the Cherenkov light, and allow for a clear discrimination between the Cherenkov and scintillation light. The preferred scintillation light is thus at a longer wavelength, and not necessarily bright nor fast. Inorganic crystals being investigated are doped lead fluoride (PbF_2) [3,26], lead chloride fluoride (PbFCl) [27–29] and bismuth silicate ($Bi_4Si_3O_{12}$ or BSO) [30–32].

Figure 20 shows UV light-excited decay kinetics of doped PbF_2 samples [26]. The decay time of rare earth-doped PbF_2 crystals is several milliseconds which is too long to be used for HHCAL. Figure 21 shows decay kinetics of PbFCl crystal excited by gamma rays. Its 24 ns decay time is appropriate for the HHCAL application. Because of the cleavage planes

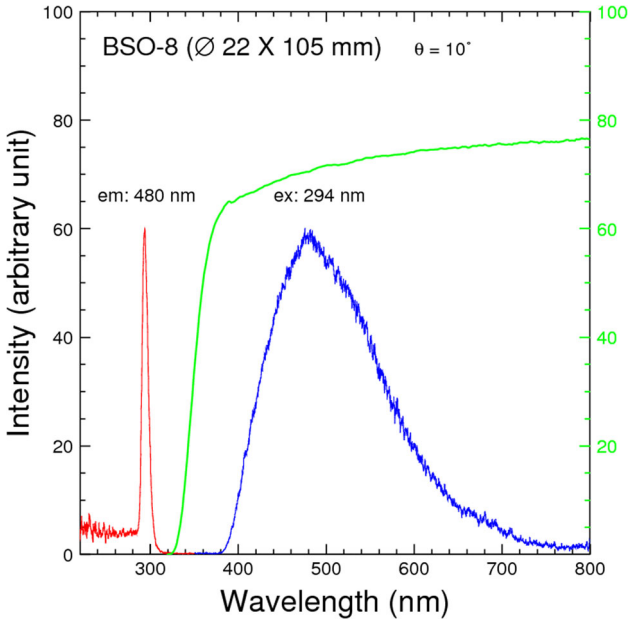

Fig. 22 LT and PL of BSO crystal

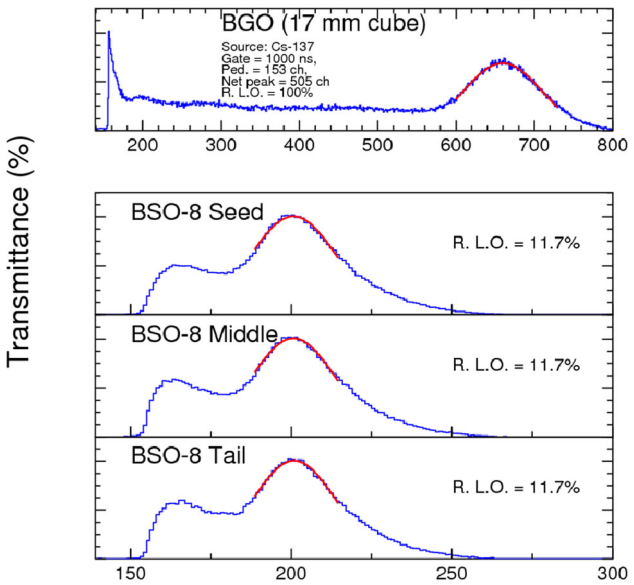

Fig. 23 Relative LO of BSO crystal

existing in its lattice structure, however, PbFCl crystal of large size is hard to grow.

Because of its low UV cutoff wavelength (300 nm) and low raw material cost (< 50% of BGO), BSO crystals are under development at SIC. Figure 22 shows longitudinal transmittance (LT) and photoluminescence (PL) spectra for a 105-mm-long BSO crystal. Figure 23 shows relative light output of the BSO crystal comparing to BGO crystal. The LO of BSO with 100 ns decay time is approximately 12% of BGO crystal. See Reference [33] for recent development for this crystal.

Summary

Bright, fast and radiation hard LYSO/LSO crystals may be used for a total absorption ECAL. LYSO/W Shashlik calorimeter was of two options for the CMS FCAL upgrade technical report for the proposed HL-LHC. Crystal calorimeters with more than ten times faster rate/timing capability require very fast crystals, e.g., sub-ns decay time of the BaF_2 fast scintillation component. Crystals (PbF_2, PbFCl and BSO) may provide a foundation for a homogeneous hadron calorimeter with dual readout for both Cherenkov and scintillation light to achieve unprecedented jet mass resolution for future lepton colliders.

Acknowledgements This work is supported by the U.S. Department of Energy, Office of High Energy Physics program under Award Number DE-SC0011925.

References

1. R.Y. Zhu, Phys. Proc. **37**, 372 (2012)
2. A. Driutti, A. Para, G. Pauletta, N.R. Briones, H. Wenzel, J. Phys. Conf. Ser. **293**, 012034 (2010)
3. R.H. Mao, L.Y. Zhang, R.Y. Zhu, IEEE Trans. Nucl. Sci. **59**, 2229–2236 (2012)
4. S. Chatrchyan, V. Khachatryan, A.M. Sirunyan, A. Tumasyan, W. Adam, E. Aguilo et al., Phys. Lett. B **716**, 30 (2012)
5. R.Y. Zhu, IEEE Trans. Nucl. Sci. **51**, 1560 (2004)
6. T. T. de. Fatis on behalf of the CMS Collaboration, J. Phys. Conf. Ser. **404**, 012002 (2012)
7. R.Y. Zhu, Nucl. Instrum. Methods A **413**, 297 (1998)
8. R.H. Mao, L.Y. Zhang, R.Y. Zhu, IEEE Trans. Nucl. Sci. **51**, 1777 (2004)
9. R. Y. Zhu, http://www.hep.caltech.edu/~zhu/talks/ryz_101209_pwo.pdf
10. G. Dissertori, D. Luckey, F. Nessi-Tedaldi, F. Pauss, M. Quittnat, R. Wallny et al., Nucl. Instrum. Methods A **745**, 1 (2014)
11. C. Biino, *in these Proceedings*
12. L.Y. Zhang, R.H. Mao, F. Yang, R.Y. Zhu, IEEE Trans. Nucl. Sci. **61**, 483 (2014)
13. C.L. Melcher, J.S. Schweitzer, IEEE Trans. Nucl. Sci. **39**, 502 (1992)
14. T. Kimble, M. Chou, B.H.T. Chai, in *Proceedings of IEEE Nuclear Science Symposium Conference*, vol 3 (Norfolk, Virginia, USA), p. 1434 (2002)
15. D.W. Cooke, K.J. McClellan, B.L. Bennett, J.M. Roper, M.T. Whittaker, R.E. Muenchausen et al., J. Appl. Phys. **88**, 7360 (2000)
16. J.M. Chen, R.H. Mao, L.Y. Zhang, R.Y. Zhu, IEEE Trans. Nucl. Sci. **54**, 718 (2007)
17. J.M. Chen, L.Y. Zhang, R.Y. Zhu, IEEE Trans. Nucl. Sci. **52**, 3133 (2005)
18. G. Eigen, Z. Zhou, D. Chao, C.H. Cheng, B. Echenard, K.T. Flood et al., Nucl. Instrum. Methods A **718**, 107 (2013)
19. G. Pezzullo, J. Budagov, R. Carosi, F. Cervelli, C. Cheng, M. Cordelli et al., J. Instrum. **9**, C03018 (2014)
20. J.M. Chen, R.H. Mao, L.Y. Zhang, R.Y. Zhu, IEEE Trans. Nucl. Sci. **54**, 1319 (2007)
21. R.H. Mao, L.Y. Zhang, R.Y. Zhu, IEEE Trans. Nucl. Sci. **59**, 2224 (2012)
22. G. Graham, C. Seez, *CMS Note 1996-002*

23. G. Pezzullo, J. Phys. Conf. Ser. **587**, 012047 (2015)
24. S.E. Derenzo, M.J. Weber, W.W. Moses, C. Dujardin, IEEE Trans. Nucl. Sci. **47**, 860 (2000)
25. R.Y. Zhu, http://www.hep.caltech.edu/~zhu/talks/ryz_110428_time_resolution.pdf
26. R.H. Mao, L.Y. Zhang, R.Y. Zhu, IEEE Trans. Nucl. Sci. **57**, 3841 (2010)
27. F. Yang, G.Q. Zhang, G.H. Ren, R.H. Mao, L.Y. Zhang, R.Y. Zhu, IEEE Trans. Nucl. Sci. **61**, 489 (2014)
28. G.Q. Zhang, F. Yang, Y.T. Wu, D.D. Sun, S.S. Shang, G.H. Ren, J. Inorg. Mater. **29**, 162 (2014)
29. J.M. Chen, D.Z. Shen, G.H. Ren, R.H. Mao, Z.W. Yin, J. Phys. D Appl. Phys. **37**, 938 (2004)
30. Y.T. Fei, S.J. Fan, R.Y. Sun, J.Y. Xu, M. Ishii, Prog. Cryst. Growth Ch **40**, 189 (2000)
31. A. Barysevich, V. Dormenev, A. Fedorov, M. Glaser, M. Kobayashi, M. Korjik et al., Nucl. Instrum. Methods A **701**, 231 (2013)
32. M. Ishii, K. Harada, N. Senguttuvan, M. Kobayashi, I. Yamaga, J. Cryst. Growth **205**, 191 (1999)
33. F. Yang, H. Yuan, L. Zhang, R.Y. Zhu, J. Phys. Conf. Ser. **587**, 012064 (2015)